# Viscous heating analysis of simulant feces by computational fluid dynamics and experimentation

Jagdeep T. Podichetty, Md. Waliul Islam, David Van, Gary L. Foutch and A. H. Johannes

## ABSTRACT

Highly viscous substances, such as feces, produce significant heat when layer deformation occurs. We describe the use of viscous heating sufficient to destroy disease-causing microorganisms and whipworms in feces. Computational fluid dynamics (CFD) was used to evaluate preliminary design and provide initial geometric specifications for a laboratory-scale unit. The laboratory device has a rotating core separated from a fixed shell wall by a defined space. Data were obtained over a range of operating conditions with simulant materials. The CFD model was validated with the experimental results. The temperature observed with the smallest spacing was 190 °C. Alternative geometries are considered for high-volume sludge processing. Potential design modifications include enhancing efficient water evaporation and recovery.

**Key words** | Comsol Multiphysics, extrusion, feces, parasite, viscosity, viscous heating

**Jagdeep T. Podichetty**
**Md. Waliul Islam**
**David Van**
**Gary L. Foutch** (corresponding author)
**A. H. Johannes**
423 Engineering North,
School of Chemical Engineering,
Oklahoma State University,
Stillwater,
OK 74078,
USA
E-mail: *foutch@okstate.edu*

## LIST OF SYMBOLS

$C_p$ specific heat capacity, J/kg K
$F$ volume force vector, N/m$^3$
$F_r$ volumetric force component radial direction, N/m$^3$
$F_\varphi$ volumetric force component rotational direction, N/m$^3$
$F_z$ volumetric force component axial direction, N/m$^3$
$k$ thermal conductivity, W/m K
$p$ pressure, Pa
$Q$ heat, J or kJ
$Q_{vh}$ viscous heat, J
$r$ radius, m
$t$ time, s
$T$ absolute temperature, K
$u$ velocity, m/s
$u'$ radial velocity, m/s
$v'$ rotational velocity, m/s
$w'$ axial velocity, m/s
$w_W$ velocity component in angular direction, m/s
$W_p$ pressure work, J

### Greek

$\rho$ density, kg/m$^3$
$\eta$ dynamic viscosity, Pa.s
$\omega$ angular velocity, m/s
$\beta$ efficiency

### Superscript

$T$ transpose

doi: 10.2166/washdev.2013.070

## INTRODUCTION

Worldwide, numerous technologies are being considered for the treatment of human wastes to minimize the spread of disease. Diarrheal diseases kill approximately 1.3 million people annually; most are children aged 0–4 years (World Health Organization 2012). Contaminated water, as a result of poor or inadequate sanitation, accounts for substantial mortality and is the leading cause of diarrhea in developing countries, especially urban slums. Fecal matter carrying pathogens can enter the water supply in multiple ways: storm water runoff, septic tank leakage, sanitary sewer system breakage and overflow, and improper disposal of human and animal waste

(Santo Domingo *et al.* 2007). Parasites that spread throughout the environment with human feces include helminths and protozoa, with particular interest focused on *Ascaris lumbricoides*, *Giardia intestinalis*, *Trichuris trichiura*, *Cryptosporidium* spp. and *Taenia* spp. (Trönnberg *et al.* 2010). In areas where sanitation is non-existent or ineffective (Trönnberg *et al.* 2010), these parasites and protozoa cause diseases such as cholera, diarrhea and typhoid. The helminth (parasitic worm) infections in the human stomach caused by the microbes listed above are ascariasis, trichuriasis (whipworm) and hookworm. These diseases cause both physical harm and reduce scholarly and cognitive development (Bethony *et al.* 2006).

Viscous heating is a well-known phenomenon; technologies include polymer melts and sludge dewatering. Rock formation is also associated with viscous heating in nature. A discussion of the contribution of viscous heating in the field of geology, along with modeling of the effects is presented by Burg & Gerya (2005). During viscous heating, temperature rise is caused by internal friction at high flow velocities (Sunden 1992). Sunden showed viscous heating effects in forced convective flow across a circular cylinder at low Reynolds numbers. To evaluate viscous heating for this application fecal simulants were used. Structural, thermal and viscoelastic properties for potatoes (Singh *et al.* 2008) indicate their potential as a simulant. Yavuz *et al.* (2011) investigated laminar duct flow heat transfer with viscous dissipation for a Newtonian fluid to define temperature distribution within annular pipes. Finite difference analysis of the heat transfer mechanisms for non-Newtonian fluids in circular tubes showed that viscous dissipation leads to high temperature in processing fluids. Heat generated decreases the viscosity of the fluid and results in less temperature rise than for a material with constant viscosity (Costa & Macedonio 2005).

We are evaluating the application of viscous heating as a component of sanitation. Heat is generated within fecal simulants by applying shear stress with an extruder. Heat generation is sufficient to sanitize the mass. For watery solids, paper, sawdust or grass clippings could potentially be added to increase viscosity. Alternatively, allowing water in the heated mass to vaporize and recycling the solids may maintain high viscosity and achieve sufficient temperature. Once treated, the feces will be safe to handle or transport and can subsequently be used in energy conversion or agricultural processes.

Similar devices for non-fecal applications have been reported; for example, Yesilata (2002) worked on the rotation of mass between two parallel disks. Hooman & Ejlali (2010) included viscous heating in a correlation to improve flow. They explained liquid viscosity decreases with incremental temperature which resulted in lower pressure drop. Although they provided a theoretical solution for both no-slip and slip flow in cases with forced convection of liquid in a micro channel flow, no experimentation was included. However, an analytical solution for nonisothermal flow with wall slip provided a better understanding of temperature rise in die flow for viscoelastic fluids (Lawal & Kalyon 1997). Their mathematical solution indicates application over a varied range of viscoplastic fluids. Depending on the resultant viscosity, a portion of the processed product might be recycled to sustain constant viscosity. Temperature distribution due to viscous heating of a shear stressed fluid is discussed by Collins (1983).

In this study, preliminary designs were evaluated using computational fluid dynamics (CFD). These simulation programs solve and analyze energy and mass balances within any geometry. For a shear reactor, these equations describe the mass flow and temperature profiles. CFD is superior to simplified approaches, such as one-dimension flow analysis methods using hydraulic radii and lubrication approximations (Gifford 1997). Results indicated initial geometric specifications prior to construction and reduced mechanical trial and error. The CFD model was validated with experimental results using fluid properties and rheology data for red potatoes. Variable analysis was performed within the CFD simulator to evaluate the effects of shear reactor geometry on temperature gradient.

## MATERIALS AND METHODS

### CFD modeling

#### Governing equations

Typically, an extruder-die design depends on three elements, an accurate viscosity model, ability to solve three-dimensional (3D) flow equations, and an objective function

to distinguish among designs. An accurate flow prediction requires a viscosity model that includes the effects of shear rate. When the viscosity correlations are unknown, the designer must define appropriate equations prior to model development. For example, most polymers behave as a Newtonian fluid at low shear rates; however, they become shear-thinning fluids under high shear force. A flow analysis requires a continuous viscosity correlation extending over the full shear-rate range observed in the analyzed fluid. The applicability of a model depends on the representation of the experimental data. When a power-law expression is not adequate, a more suitable model, such as those by Carreau-Yasuda, Bird-Carreau and Cross, may be required (Gifford 1997; Vlachopoulos & Strutt 2003).

Comsol Multiphysics v4.2a (C-M) – a commercial CFD package – was used to analyze the temperature profile within the reactor geometries (COMSOL MULTIPHYSICS 2011). C-M can handle steady state, transient flow with heat equations using finite element algorithm in both two-dimensional (2D)and 3D geometries. The flow is governed by the time-dependent Navier–Stokes equations. Equation (1) represents the vector form of the conservation of momentum equation and Equation (2) is the continuity equation for the conservation of mass. The heat transfer in the fluid domain is described by Equations (3) through (5).

$$\rho\frac{\partial u}{\partial t}+\rho(u.\nabla)u=\nabla\cdot[-pI+\ \eta(\nabla u+(\nabla u)^{\mathrm{T}}]+F \tag{1}$$

$$\rho\nabla.u=0 \tag{2}$$

$$\rho C_p\frac{\partial T}{\partial t}+\rho C_p u.\nabla T=\nabla\cdot(k\nabla T)+Q+Q_{vh}+W_p \tag{3}$$

$$Q_{vh}=\mu\left(\nabla u+(\nabla u)T-\left(\frac{2}{3}\right)(\nabla.u)I\right):\nabla u \tag{4}$$

$$W_p=\frac{T}{\rho}\left(\frac{\partial\rho}{\partial t}\right)_p\left(\frac{\partial p_A}{\partial t}+u.\nabla p_A\right) \tag{5}$$

The terms $Q_{vh}$ and $W_p$ are added to the general heat-transfer equation to include viscous heating and pressure work effects. All three velocity components must be included in the model since the velocities in the angular direction are different. The flow Equations (6) through (8) for a stationary axi-symmetric geometry are described by Gresho & Sani (1998):

$$\rho\left(u'\frac{\partial u}{\partial r}-\frac{v'2}{r}+w'\frac{\partial u}{\partial z}\right)+\frac{\partial p}{\partial r}=\eta\left[\frac{1}{r}\frac{\partial}{\partial r}\left(r\frac{\partial u'}{\partial r}\right)-\frac{u'}{r^2}+\frac{\partial^2 u'}{\partial z^2}\right]+F_r \tag{6}$$

$$\rho\left(u'\frac{\partial v'}{\partial r}+\frac{u'v'}{r}+w'\frac{\partial v'}{\partial z}\right)\ =\eta\left[\frac{1}{r}\frac{\partial}{\partial r}\left(r\frac{\partial v'}{\partial r}\right)-\frac{v'}{r^2}+\frac{\partial^2 v'}{\partial z^2}\right]+F_\varphi \tag{7}$$

$$\rho\left(u'\frac{\partial w'}{\partial r}+w'\frac{\partial w'}{\partial z}\right)+\frac{\partial p}{\partial r}\ =\eta\left[\frac{1}{r}\frac{\partial}{\partial r}\left(r\frac{\partial w'}{\partial r}\right)+\frac{\partial^2 w'}{\partial z^2}\right]+F_z \tag{8}$$

In this study, the effect of body force components of the momentum equation are assumed negligible. Hence, for this model the volumetric force components $F_r$, $F_\varphi$ and $F_z$ are set to zero. The velocity components in the plane are zero. The velocity components in the angular direction are computed by Equation (9).

$$w_W=r\omega \tag{9}$$

## Model geometry

We describe how CFD is used to devise a shear reactor that would disinfect human feces by performing a variable analysis. With experimental data the CFD model can be fine-tuned for additional analysis. The reactor geometry is rotationally symmetric (Figure 1) and can be setup with a 2D cross-section and extended to the original 3D geometry. At the outer cylinder wall a no-slip condition applies. Initial conditions of 0 Pa and

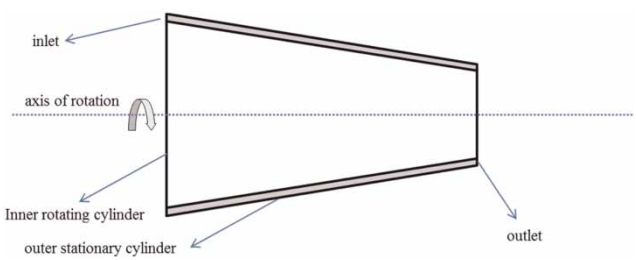


**Figure 1** | Reactor geometry used for CFD studies.

298 K are used. The thermal properties of high-strength alloy steel were used for the reactor geometry. The outside surface of the reactor was set to free convection with a heat transfer coefficient of 5 W/m$^2$ K. The angle of the extruder allows multiple spacing tests with a single experimental device. By fixing the shell and moving the core axially the spacing can be adjusted.

The geometry was meshed using an interactive technique. A total of 454,902 domain nodes and 3,510 boundary nodes were created within a mesh area of 0.0032 m$^2$ for the 2D cross-section. The 2D cross-section was rotated around the axis of rotation to obtain the full 3D profile. A grid dependency test was performed to determine the optimum number of grid nodes. Increasing the number of nodes altered the temperature predictions less than 0.4%. Hence, the number of nodes was considered optimum. Table 1 shows the properties used for simulations. The viscosity model for red potato was developed from experimental rheology data and was used to validate the CFD model. The simulations were performed with stationary 'Fully Coupled' solver configuration. A Parallel Sparse Direct Solver was used to obtain simulation results. To validate the CFD model, experiments were performed, as described in the next section, at various operating conditions.

**Table 1** | Properties used for CFD modeling

| | |
|---|---|
| *Red potato* | |
| Density, $\rho$ | 1,030 kg/m$^3$ |
| Viscosity model, $\mu$ | 0.4 Pa s; $t = 0$ s<br>206.4*(Shear rate)$^{-0.92}$ Pa · s; $t > 0$ s |
| Thermal conductivity, $k$ | 0.03 W/(m K) |
| Heat capacity, $C_p$ | 4,186 J/(kg K) |
| *High-strength alloy steel* | |
| Head capacity, $C_p$ | 475 J/(kg K) |
| Thermal conductivity, $k$ | 44.5 W/(m K) |
| Density, $\rho$ | 7,850 kg/m$^3$ |

## Experimental methods

### Rheology studies

In order to measure the viscosity of different types of potatoes and wheat flour, we used a rheometer from Bohlin Instruments Model CVOR 200, East Brunswick, NJ. A sample was placed in a plastic cup within a ball mill of a THINKY grinder from Phoenix Equipment, Rochester, NY to create a paste. A 2.5 ml sample by syringe was passed inside the serrated cylinder within the rheometer. The experiment used a 150 μgap and 40 °C. The composition of simulant stool is given in Table 2 (Susana.org 2008). Based on these data, we selected red potato as our fecal simulant. To prepare feed to operate the extruder, red potatoes were boiled for at least one hour. After 10–15 min, the skin was removed and potatoes were mashed in a ricer.

**Table 2** | Composition of simulant stool

| Ingredient | Percentage |
|---|---|
| Salt | 12.2 |
| Rice | 18.5 |
| Soy bean paste | 33.8 |
| Water | 35.5 |

### Shear reactor setup and operation

The viscous heating unit is shown in Figure 2. The machine operates with a variable pressure (0–690 kPa) for feed rate control, spacing (0.75–1.25 mm) between the rotating inner core and the fixed outer shell and rotations per minute (rpm) (0–1,800). For typical operation, the room temperature is assumed constant and feed occupies the spacing completely. The simulant mass is placed inside the feed chamber, the spacing is adjusted, pressure and rpm are set and the extruder is activated. An electric switch opens the air valve and moves the plunger that pushes simulant or feces into the gap. Once some initial mass was observed to exit the shell, a rubber stop cork was used to close the outlet for a time (holdup time) to allow the equipment and the mass to heat due to friction. After the desired temperature is achieved the stopcock is removed and mass flow is established. The mass in the annular space has a defined holdup time. During experimentation temperature is recorded by a thermocouple – an Omega HHM 31 Digital Multimeter – and rpm by a digital photo laser tachometer (non-contact). Air pressure, spacing, rpm and torque data are collected.

**Figure 2** | Instrumented reactor to process fecal and simulant solids.

The plunger on the left in Figure 2 moves inside a cylindrical feed chamber to press the feed inside the shell. A hole on the cylindrical chamber allows the operator to charge the feed. The plunger is air driven and can push the feed with a gauge pressure from 0 to 100 psi. In the figure, the pressure gauge is hanging on the metallic vertical wall. Below the gauge, a regulator controls the pressure. On the right side of Figure 2, a Hitachi WJ200 Series 200 V three-phase inverter is attached on the vertical wall to set the required rpm of the AC motor.

Not shown in Figure 2, but mounted on the wall power supply, is a wattmeter to measure the energy consumption. By recording the instantaneous power a plot with time for both no-load and load operating conditions allows for calculation of the energy input into the simulant.

The cone and the shell are shown in the lower center of Figure 3. The fixed shell has a spacing calibration ranging from 0 to 1.25 mm. The cone moves inside the shell. In contact with the inner cone surface, mass starts rotating, deforms, and creates friction. The moveable bearing is attached around the stem of the cone with a black circular plastic rubber seal. The combination aligns the cone in a concentric position inside the cylindrical shell. The black hole shown on the shell in Figure 3 serves as an outlet. The shell was calibrated for three positions: 0.75, 1.00 and 1.25 mm. Spacing between the rotating cone and the stationary shell is fixed by the operator. A handle is moved to set the desired spacing based on the calibration. The spacing between the housing and rotating shaft is increased if the metal handle is pushed forward to the vertical metal wall (anticlockwise direction as you look from

**Figure 3** | The cone (left) rotates inside the housing (right).

the side of the air cylinder inlet). Vegetable dye tracer studies confirmed plug flow behavior through the reactor.

## RESULTS AND DISCUSSION

### Shear rate dependency on viscosity

Finding a reasonable and safe simulant for experimentation was required. A search of shear thinning fluids (where viscosity decreases with increasing shear rate) indicated several alternatives with similar properties to feces. Figure 4 presents viscosity data for pig caecal, chicken caecal and human stool compared with several starchy materials and simulant stool (Doucleff 2012). The viscosity decreased with increase in shear rate. The graphical representation for fecal matter follows a similar trend line (Woolley *et al.* 2013). Plots of the same type are found for wheat and maize starch paste in Ellis *et al.* (1989). While wheat flour had the closest match with human feces over a range of shear rate, red potatoes were selected as the test simulant when matched with moisture content and ease of preparation.

### Viscous heating of simulant (red potato) and CFD model validation

As the core rotates inside the housing, the potatoes pass between the two metallic surfaces. The outlet was closed for a certain holdup time and the potatoes gained heat. When allowed to exit the reactor, the elevated temperature observed initially reduces as the mass cools due to water evaporation and release to atmospheric pressure. Table 3 shows data for experiments at 1,800 rpm with a spacing of

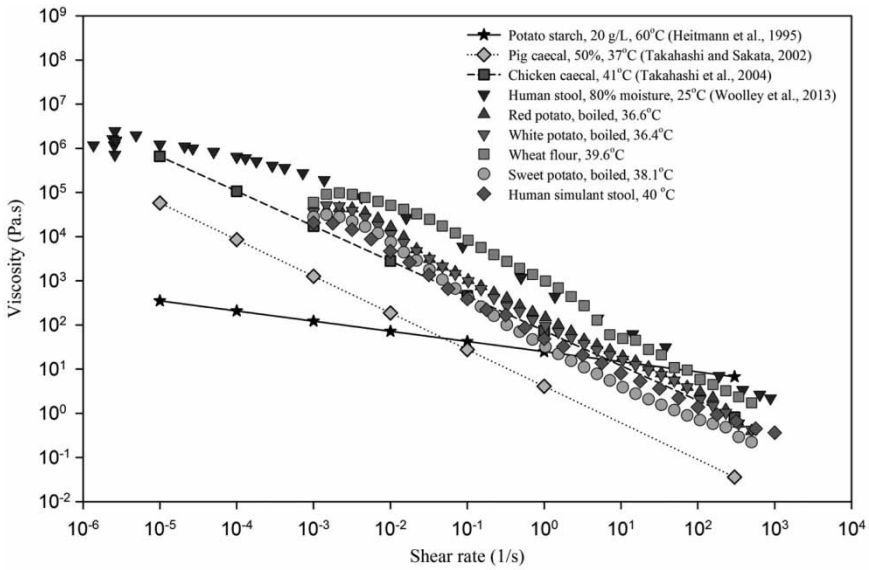


**Figure 4** | Shear rate decrease with viscosity for various feces and simulants.

**Table 3** | CFD and experimental results: Temperature with time at constant feed pressure, rpm and spacing

| Feed | Pressure kPa | rpm | Spacing mm | Holdup time seconds | Temperature outlet °C | CFD average fluid temperature °C |
|---|---|---|---|---|---|---|
| Red potato | 690 | 1,800 | 0.75 | 0 | 34 | 35 |
| | | | | 60 | 64 | 76 |
| | | | | 120 | 74 | 103 |
| | | | | 180 | 86 | 131 |
| | | | | 240 | 162 | 159 |
| | | | | 260 | 190 | 168 |

0.75 mm and feed pressure of 690 kPa at various holdup times. As the holdup time increased, the temperature increased.

The temperature increased with holdup time. A temperature of 190 °C was obtained at 260 s holdup time. Experiments were stopped at this temperature to prevent excessive wear and tear on the equipment. This temperature exceeded that required to kill all microorganisms in human feces by thermal energy alone. However, additional microbial destruction is anticipated from the shear stress within the extruder. Temperatures for steam sterilization required 121 °C for 30 min or 132 °C for 4 minutes (Rutala & Weber 2008).

Figure 5 presents results for experiments with the reactor feed pressure at 690 kPa, 1,800 rpm and 0.75 mm spacing. We performed additional experiments – not presented – at constant rpm and spacing and found a similar trend. The maximum temperature in Figure 5 shows the limitations of the equipment. We believe that increasing rpm and decreasing spacing would increase temperature further. Additional experimentation on the destruction of microbes was performed and is presented in a companion paper.

The data for various holdup times was used to validate the CFD model. Table 3 compares CFD results with data at the same conditions. The CFD results in Figure 5 indicate a linear increase in temperature with holdup, suggesting that increasing hold time would increase fluid temperature. The deviation between CFD predictions and experimental measurements can be attributed to the thermal mass of the system, heat loss and temperature measurement technique. An average fluid temperature was obtained from CFD while outlet temperature was measured during experiments. A maximum temperature of 218 °C was predicted by CFD simulations. Figure 6 shows the fluid temperature profile at 260 s. The CFD model can be used effectively to make improvements to the current design. Experiments were also performed by varying reactor spacing at constant pressure, rpm and holdup time.

Table 4 indicates that temperature decreases with increased spacing. These results suggests the likelihood that lower spacing, less than 0.75 mm, will generate even higher temperature. However, the temperature requirements to kill microorganisms have been achieved; hence, further reduction was unnecessary. The experiments were done at constant feed pressure of 690 kPa, 1,209 rpm and 180 s holdup time. After 180 s, the rubber stop cork was removed and the mass was allowed to leave to the environment. The

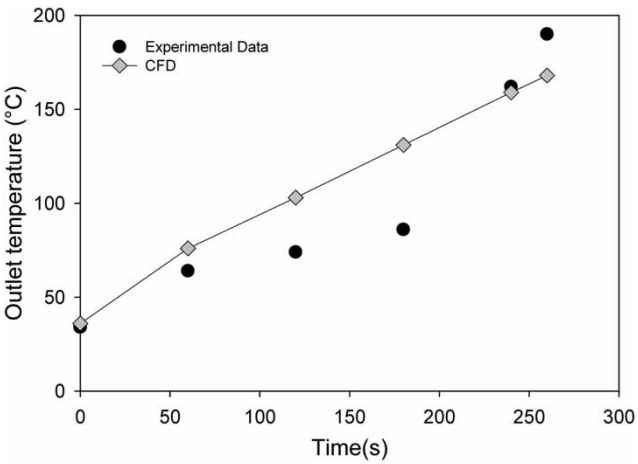


**Figure 5** | Average fluid temperature from CFD and outlet temperature from experimental measurements at 1,800 rpm and 0.75 mm reactor spacing.

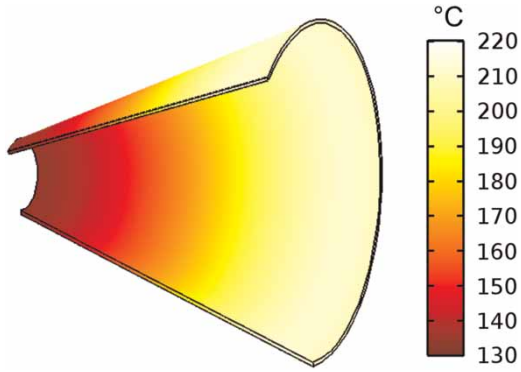


**Figure 6** | CFD fluid temperature profile: red potato at 260 s holdup time.

**Table 4** | Temperature data with the change of spacing at constant pressure, rpm and holdup time

| Feed | Pressure kPa | rpm | Holdup time seconds | Spacing mm | Temperature outlet °C |
|---|---|---|---|---|---|
| Red potato | 690 | 1,209 | 180 | 0.75 | 72 |
| | | | | 1 | 70 |
| | | | | 1.25 | 50 |

**Table 5** | Temperature with rpm change at constant pressure, holdup time and spacing

| Feed | Pressure kPa | Spacing mm | Holdup time seconds | rpm | Outlet temperature °C |
|---|---|---|---|---|---|
| Red potato | 690 | 0.75 | 180 | 913 | 55 |
| | | | | 1,209 | 72 |
| | | | | 1,504 | 104 |

mass was observed to be hot, moist, and dried quickly when exposed to air.

In the next attempt, the effect of rpm on temperature rise is evaluated (Table 5). We see at 690 kPa feed pressure, 0.75 mm spacing, and 180 s holdup time, that the temperature rises linearly.

While 120 °C is sufficient to sanitize the waste, operation at higher temperature supplies additional energy with the primary benefit being increased water evaporation rate. The 'cost' for the additional temperature depends on equipment and utility costs. The operation conditions must be based on optimization of these operational (energy cost) and capital (equipment wear) factors. In summary, higher holdup time, lower spacing and higher rpm enhance outlet temperature.

## Effect of dimension

To evaluate the reactor geometry, the length, angle of the cone and clearance were varied to define the effect of dimensions on temperature gradient. The temperature profiles in Figure 7 show an increase in average fluid temperature with greater length. Higher temperatures were observed at the larger section of the reactor. An average fluid temperature of 114, 168 and 225 °C was obtained for reactor lengths 0.05, 0.1 and 0.15 m, respectively. Increase in average fluid temperature was caused by increase in surface area for the same amount of feed. The change in angle of the cone follows the same trend as changes in length. Increasing the angle of the cone increases surface area and viscous heating. A smaller clearance results in higher maximum temperature, reducing the clearance from 0.75 to 0.5 mm increased the average fluid temperature by 68 °C.

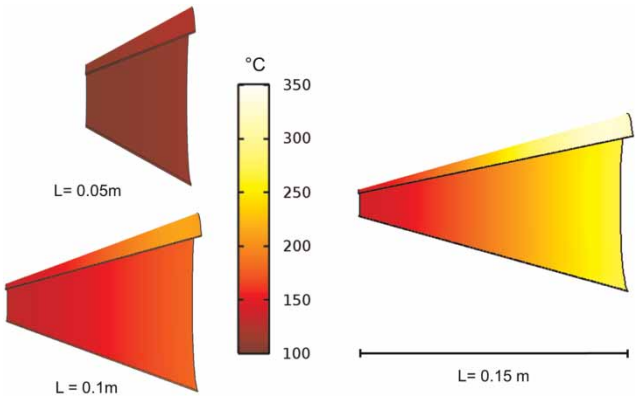


**Figure 7** | CFD average fluid temperature profile: the effect of length (L).

An increase in angular velocity increases viscous heating significantly. An average temperature of 168, 127 and 76 °C was obtained at 1,800, 1,000 and 500 rpm, respectively. The velocity component in the angular direction (Equation (9)) decreases with decrease in length for the reactor, resulting in relatively larger surface area for the fluid in the larger section of the reactor with corresponding higher temperature.

## Shear reactor energy balance

The wattmeter installed in the power supply line to the reactor motor was used to measure the energy consumption. Potatoes were charged to the reactor and the experiment operated at 690 kPa feed pressure, 0.75 mm gap spacing and 1,800 rpm setting with a holdup time of 260 s (time to achieve 190 °C per Table 3) for two different conditions – with and without feed into the reactor. For both cases, power consumption was recorded every 10 s. A plot of instantaneous power versus time was obtained for both no load and load conditions (Figure 8). Energy input to the feed was calculated by subtraction.

The area under the power versus time curve (Figure 8) gives the total energy consumed. For a 260 s run, the energy with load was 243 kJ, and without load was 172 kJ; for a difference of 71 kJ. Most of the energy input to the simulant occurs in the first 90 s and then drops to a near steady state value as viscosity is reduced. Correspondingly, temperature increases rapidly initially and then climbs gradually, nearly at steady state. Some energy is retained by the mass, but most is conducted through the metal shell and core. If the experiments are stopped at 90 s, 48% of the energy input would go to viscous energy of the mass and most of that energy would transfer out of the reactor

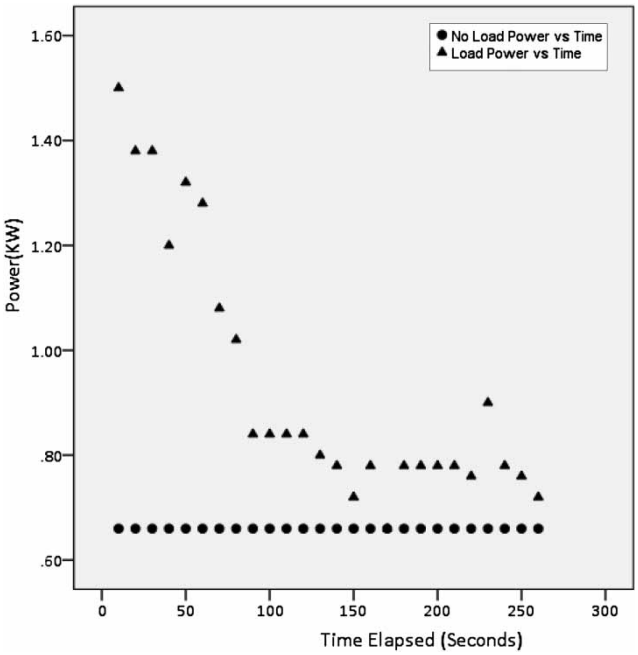


**Figure 8** | Power versus time for no load and load conditions at 690 kPa, 0.75 mm spacing and 1,800 rpm.

by conduction. The longer the system runs at steady state, the lower the percentage of total energy goes into the simulant. By the end of the full 260 s run the total fraction of energy input into the simulant was 29%. Clearly, if viscous heating is the goal then the device should be well insulated and stopped as soon as the required temperature is achieved. In design, for a given rpm and geometry the simulant flow rate can be established for a fixed percentage power input between 29 and 48%. However, if a specific temperature is required then a singular efficiency will result for a specific material and system geometry.

## CONCLUSIONS

CFD studies showed the temperature gradient in the reactor depends significantly on the angular velocity, inlet velocity, spacing and extruder length. The CFD model was validated with experimental data. Experimentation confirmed that viscous heating by extrusion may be effective in decontaminating fecal wastes. For each experiment, fixing two variables from among rpm, holdup time and gap spacing allowed one variable to be compared with the resulting temperature change. Temperature was observed to increase with decreasing spacing, increasing rpm and increasing contact time. The maximum temperature achieved was 190 °C within 3–4 min with red potatoes. An insulated system would ensure the desired temperature in the shortest time and, in turn, higher mass throughput for a specific temperature and geometry. A significant factor is the requirement of high viscosity to generate heat. For cases where people have diarrhea, where urine is not separated or when water is added, this technology will require feed mass modification to increase viscosity. Possibilities include the addition of paper or biomass, or design modifications that includes recycle of some of the dried solid waste. By balancing the ratio of recycle to fresh feed the required viscosity can be achieved.

## ACKNOWLEDGEMENT

The authors would like to thank Mr Ronny E. Markum of the Advanced Technology Research Center, Oklahoma State University for assisting with the design, building the equipment and troubleshooting the operation. This work was supported by the Bill & Melinda Gates Foundation through a Grand Challenges Explorations grant.

## REFERENCES

Bethony, J. S., Brooker, M., Albonico, S. M., Geiger, A., Loukas, D., Diemert, R. J. & Hotez, P. J. 2006 Soil-transmitted helminth infections: ascariasis, trichuriasis, and hookworm. *The Lancet* **367** (9521), 1521–1532.

Burg, J. P. & Gerya, T.V. 2005 The role of viscous heating in Barrovian metamorphism of collisional orogens: thermomechanical models and application to the Lepontine Dome in the Central Alps. *Journal of Metamorphic Geology* **23** (2), 75–95.

Collins, M. W. 1983 A finite difference analysis for laminar heat transferr of non-newtonian fluids in circular tubes. *Numerical Methods in Thermal Problems*, Volume 3 – Proceedings of the Third International Conference, Seattle, WA, August 2–5, 1983, pp. 540–550.

COMSOL MULTIPHYSICS 2011 *COMSOL Multiphysics User's Guide.* Stockhlom, Sweden: Version 4.2a.

Costa, A. & Macedonio, G. 2005 Viscous heating effects in fluids with temperature-dependent viscosity: triggering of secondary flows. *Journal of Fluid Mechanics* **540**, 21–38.

Doucleff, M. 2012 Why is the world's largest foundation buying fake poop? www.npr.org/blogs/health/2012/08/08/158447235/why-is-the-worlds-largest-foundation-buying-fake-poop (Accessed: 25 August 2013).

Ellis, H. M., Ring, S. G. & Whittam, M. A. 1989 A comparison of the viscous behaviour of wheat and maize starch pastes. *Journal of Cereal Science* **10**, 33–44.

Gifford, W. A. 1997 The use of three dimensional computational fluid dynamics in design of extrusion dies. *Journal of Reinforced Plastics and Composites* **16**, 661–674.

Gresho, P. M. & Sani, R. L. 1998 *Incompressible Flow and the Finite Element Method, Volume 2, Isothermal Laminar Flow*. Wiley, New York.

Hooman, K. & Ejlali, A. 2010 Effects of viscous heating, fluid property variation, velocity slip, and temperature jump on convection through parallel plate and circular microchannels. *International Communications in Heat and Mass Transfer* **37** (1), 34–38.

Lawal, A. & Kalyon, D. M. 1997 Viscous heating in nonisothermal die flows of viscoplastic fluids with wall slip. *Chemical Engineering Science* **52** (8), 1323–1337.

Rutala, W. A. & Weber, D. J. 2008 *Guideline for Disinfection and Sterilization in Healthcare Facilities*. CDC, USA.

Santo Domingo, J. W., Lu, J., Shanks, O. C., Lamendella, R., Kelty, C. A. & Oerther, D. B. 2007 Development of host-specific metagenomic markers for microbial source tracking using a novel metagenomic approach. *Disinfection* **16**, 646–661.

Singh, N., Isono, N., Srichuwong, S., Noda, T. & Nishinari, K. 2008 Structural, thermal and viscoelastic properties of potato starches. *Food Hydrocolloids* **22** (6), 979–988.

Sunden, B. 1992 Vicous heating in forced convective heat-transfer across a circular-cylinder at low reynolds-number. *International Journal for Numerical Methods in Engineering* **35** (4), 729–736.

SuSanA – Sustainable Sanitation Alliance 2008 MISO (Soybean Paste) 14 March 2008. http://forum.susana.org/media/kunena/attachments/52/certificate.pdf (Accessed: 03 June 2012).

Trönnberg, L., Hawksworth, D., Hanses, A., Archer, C. & Stenstrom, T. A. 2010 Household-based prevalence of helminths and parasitic protozoa in rural KwaZulu-Natal, South Africa, assessed from faecal vault sampling. *Transactions of the Royal Society of Tropical Medicine and Hygiene* **104** (10), 646–652.

Vlachopoulos, J. & Strutt, D. 2003 The Role of Rheology in Polymer Extrusion. *New Technologies for Extrusion Conference*, Milan, Italy.

Woolley, S., Buckley, C., Pocock, J., Cottingham, R. & Foutch, G. 2013 Some rheological properties of fresh human feces with a variation in moisture content & Rheological modeling of fresh human feces. *3rd SA YWP Conference*, Stellenbosch, Western Cape, South Africa.

World Health Organization 2012 Water, sanitation and hygiene links to health. www.who.int/water_sanitation_health/publications/facts2004/en/ (Accessed: 12 Sep 2012).

Yavuz, T., Erol, O. & Kaya, M. 2011 Heat transfer characteristics of laminar annular duct flow with viscous dissipation. *Proceedings of the Institution of Mechanical Engineers Part C-Journal of Mechanical Engineering Science* **225** (C7), 1681–1692.

Yesilata, B. 2002 Viscous heating effects in viscoelastic flow between rotating parallel-disks. *Turkish Journal of Engineering & Environmental Sciences* **26** (6), 503–511.

First received 6 May 2013; accepted in revised form 5 September 2013. Available online 21 October 2013